RSC Advances

ROYAL SOCIETY OF CHEMISTRY

PAPER

View Article Online
View Journal | View Issue

Cite this: *RSC Adv.*, 2021, **11**, 25752

Bioinspired triangular ZnO nanoclusters synthesized by *Argyreia nervosa* nascent leaf extract for the efficient electrochemical determination of vitamin C†

Pooja Singh, [a] Kshitij RB Singh, [b] Jay Singh, [c] Priyanka Prasad [d] and Ravindra Pratap Singh *[a]

Received 17th June 2021
Accepted 11th July 2021

DOI: 10.1039/d1ra04704c

rsc.li/rsc-advances

This work deals with the synthesis of bioinspired triangular ZnO nanoclusters (bT-ZnO NCs) from *Argyreia nervosa* nascent leaf extract for their effective antibacterial activity and further utilization as a platform for the electrocatalytic determination of ascorbic acid (AA; vitamin C) for applications in the agricultural domain. The structural, optical, and morphological characteristics of the synthesized bT-ZnO NCs were analyzed by UV-vis, FT-IR, XRD, AFM, SEM, TEM, HR-TEM, and EDX techniques. After this, bT-ZnO NCs were electrophoretically deposited onto an indium-tin-oxide (ITO) glass substrate and assessed for the electro-oxidation of AA by cyclic voltammetry (CV), and from this it was proven that bT-ZnO NCs had a very high electrochemical sensitivity of 29.88 μA cm^{-2} toward AA and a low limit of detection of 0.5321 mM under the optimized experimental conditions. Thus, it provides a potential sensing platform for electrochemical studies to detect AA. Moreover, bT-ZnO NCs were preliminarily investigated for their antibacterial activity, and the obtained results showed that the bT-ZnO NCs have potency as an antibacterial agent.

1. Introduction

Over the past decade, there have been interdisciplinary fields including nanoscience and nanotechnology, interspersing material science, bionanosciences, and biotechnology. The synthesis of metal oxide nanoparticles is an important subject of research in modern physics due to their extraordinary capabilities in the fields of electronic, magnetic, optoelectronic, information storage, and drug delivery.[1–4] Nanoparticles of different shapes and sizes have been the subject of great interest due to their possible applications including industries, biomedical diagnostics, environmental remediation, and electronics. Both metal and metal oxide nanoparticles show a large surface volume ratio and are considered the most promising and remarkable agents in the agricultural domain. Recently, zinc oxide (ZnO) nanoparticles have shown various applications for addressing physical, chemical, and environmental issues and have also provided various solutions for solving problems pertaining to biological sciences. Moreover, chemical and physical methods can be used to synthesize nanoparticles, but they tend to be expensive, harmful to the environment, and need high energy consumption. Thus, biological synthesis routes utilizing various plant extracts, enzymes, and microorganisms, such as bacteria and fungi, have been suggested as possible environmentally friendly alternative methods over chemical and physical methods.[5–8] Moreover, the synthesis of nanoparticles utilizing plant extracts is more beneficial than other biological processes as plant organs are more stable, environmentally friendly, show a higher yield of nanoparticles, and are faster than the single-step biosynthesis process.[9] The plant extracts consist of various flavonoids, alkaloids, and proteins, which help in the non-agglomeration and stabilization of nanoparticles.[10–12] It has also been observed that some plants readily uptake and reduce metal ions from salt or mineral-rich soil by the process of detoxification and can convert them into nanoparticles.[13] Numerous reports are available on the plant-mediated synthesis of metallic nanoparticles, notably from *Anisochilus carnosus*, *Trifolium pratense*, *Magnolia cobus*, *Mangrera indica*, *Pomegranate*, *Calotropis gigantine*, *Annona squamosa*, *Argyreia nervosa* (*AN*), and extracts of coriander seeds; the plant-mediated synthesis of nanoparticles is

[a]*Department of Biotechnology, Faculty of Science, Indira Gandhi National Tribal University, Amarkantak, Madhya Pradesh (484886), India. E-mail: rpsnpl69@gmail.com; ravindra.singh@igntu.ac.in; Tel: +91-91-0934-6565*

[b]*Department of Chemistry, Govt. V. Y. T. PG Autonomous College, Durg, Chhattisgarh, India*

[c]*Department of Chemistry, Institute of Science, Banaras Hindu University, Varanasi, Uttar Pradesh (221005), India*

[d]*Department of Botany, Faculty of Science, Indira Gandhi National Tribal University, Amarkantak, Madhya Pradesh (484886), India*

† Electronic supplementary information (ESI) available. See DOI: 10.1039/d1ra04704c

attracting a lot of attention nowadays due to the unique properties exhibited by the nanoparticles synthesized from this route.[14–16] Moreover, biogenic metal/metal oxide-based nanoparticles have a wide range of utility in various fields, and in agriculture, where they are widely used as an antimicrobial agent, for monitoring the plant stress condition, and for the detection of effluents (pesticides, byproducts in pesticides (hydrazine), *etc.*) produced from erroneous agricultural practices.[17–20]

AN is an Indian-origin plant belonging to the Convolvulaceae family and is commonly known as morning glory. The white, dense hair under the heart-shaped leaves is the main characteristic feature of this plant. Traditionally, its roots are mainly used to treat neurodegenerative diseases, eczema, swellings, boils, ringworms, and anti-rheumatic.[21] A variety of secondary metabolites, namely glycosides, alkaloids, steroids, flavonoids, and similar active metabolites, are found in the plant, which helps them exhibit various medicinal properties, mainly anti-asthmatic, anti-inflammatory, and immune-boosting activities.[22] The presence of flavonoids also helps the plant exhibit anti-cancer activity;[23] as previously reported, *AN* can be used to synthesize silver nanoparticles.[24] Zinc oxide is an inorganic compound that is white in appearance and is insoluble in water. The white powdered form of ZnO is highly utilized in the form of additives in many materials and products, namely glass, ceramics, rubber, cement, paint, plastics, lubricants, adhesives, plasters, sealants, pigments and food, batteries, ferrite, and fire retardants. ZnO is a zincite mineral commonly found in the Earth's crust, but ZnO is produced artificially for commercial use. It plays a crucial role as one of the essential microelements in the human body.[25] It is found in the human body in different percentages, like 85% in the whole body, 11% in the skin, and is also present in other parts of the body.[26] Zinc oxide exhibits various unique chemical, optical, electric conductivity, semiconducting, and piezoelectric properties that helps it play an important role in maintaining the proper functioning of several macromolecules and enzymes for their catalytic and structural activity.[27]

Moreover, zinc oxide is also highly essential for the proper functioning of various metalloproteins. The unique scaffolding of zinc finger motifs makes the protein sub-domains interact with DNA or other proteins.[28] To date, many researchers have synthesized nanostructured ZnO, ZnO metal hybrid composites (with zinc sulfide (ZnS) and many others), and ZnO nanocomposites with drugs (like leucovorin, *etc.*) for demonstrating their potential as a photocatalyst for dye (methylene blue, eosin, *etc.*) degradation and as an anti-cancer agent to treat breast cancer and several other types of cancer.[29–31] Nowadays, nanomaterials' unique properties have led researchers to design several simple and cost-effective techniques to synthesize nanostructures of technologically beneficial materials. ZnO is considered one of the most highly explored materials in nano dimensions due to its wide bandgap and large excitonic binding energy, which are beneficial for research and industrial applications.[32] Zinc and zinc oxide are very active elements and are considered strong reducing agents that can be easily oxidized and form oxides according to their reduction potential; this property is very helpful for preparing ZnO nanoparticles.[33]

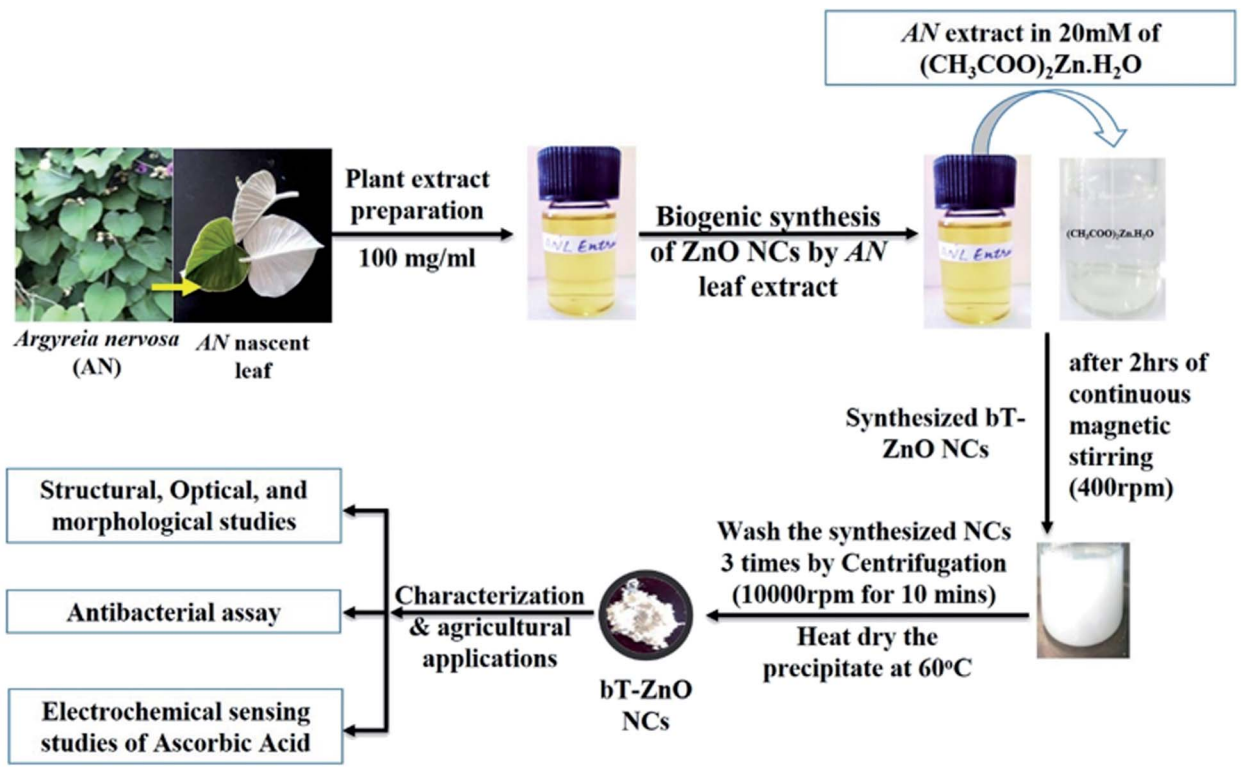

Fig. 1 Illustration presenting the complete overview of this work.

Thus, in this study (see Fig. 1 for an overview of the study), we report the synthesis of bioinspired triangular ZnO nanoclusters (bT-ZnO NCs) from *AN* nascent leave extract and their real-life application in the agricultural domain for the label-free detection of ascorbic acid (AA; vitamin C) to monitor the stress conditions in the plant and also for combating the bacterial blight disease in rice crops. Hence, this work explores the extraordinary potential of bioinspired zinc oxide nanoclusters for the label-free electrochemical sensing of AA; as for the determination of AA, labeled optical sensors that use ascorbate oxidase enzyme are available but they are costly, and so for cost reduction AA sensing, our fabricated direct sensing method can be an alternative. Apart from the sensing aspect, our study also tried to explore the antibacterial potentiality of the synthesized bT-ZnO NCs to prove their capability as a potent agent to combat a very common rice pathogen that causes bacterial blight disease and reduces the yield of rice.

2. Experimental

2.1. Material

Zinc acetate dihydrate ($(CH_3COO)_2Zn\cdot H_2O$; MW: 219.49 g mol^{-1}; CAS number: 5970-45-6), L-ascorbic acid ($C_6H_8O_6$; MW: 176.12 g mol^{-1}; Product cat no.: 50-81-7), potassium hexacyano ferrate(II) trihydrate ($C_6FeK_4N_6\cdot 3H_2O$; MW: 422.39 g mol^{-1}; Product cat no.: 1.93686.0521), potassium hexacyano ferrate(III) ($C_6FeK_3N_6$; MW: 329.25 g mol^{-1}; Product cat no.: 1.93667.0521), sodium chloride (NaCl; MW: 58.44 g mol^{-1}; Product cat no.: S9888), and Whatman filter paper Grade-1 were obtained from Sigma-Aldrich. Sodium hydroxide (NaOH; MW: 40.00 g mol^{-1}; CAS no.: 1310-73-2) and ammonia liquor (NH_3; MW: 17.03 g mol^{-1}; CAS no.: Q16225) were obtained from Qualigens, Thermo Fisher Scientific. Luria Bertani Agar, Miller (GM1151), ampicillin (SD002), disodium phosphate ($Na_2HPO_4\cdot H_2O$; MW: 177.99; CAS no.: 10028-24-7), and monosodium phosphate (NaH_2PO_4; MW: 119.98; CAS no.: 7558-80-7) were procured from Himedia. All the chemicals used for the experiments were of analytical grade and used as received without further purification. The ITO sheets (surface resistivity 30–60 Ω sq^{-1}) were procured from Sigma-Aldrich for the electrophoretic deposition of bioinspired triangular ZnO nanoclusters (bT-ZnO NCs). The pure cultures of *Escherichia coli* and *Xanthomonas oryzae* bacteria were laboratory obtained. *AN* nascent leaves were collected from the herbal garden of Dr Singh at IGNTU, Amarkantak, M.P., India. Milli-Q water (18 Ω resistivity; Millipore, USA) was used to in all the experimental works.

2.2. Preparation of the *AN* plant extract

The collected *AN* nascent leaves were washed with Milli-Q water and dried using absorbent paper; then, they were chopped into fine pieces using a sterilized chopper. Further, the finely chopped leaves were weighed for preparing the plant extract solution in Milli-Q water by adding 100 mg ml^{-1}; then, this solution was boiled for 30 min at 65–70 °C. After 30 min boiling, the extract solution was kept at room temperature. Finally, the cooled solution was centrifuged at 10000 rpm for 10 min, then the pellet was discarded, and the supernatant was retained. Further, the supernatant was filtered through the Whatman filter paper 1, and the obtained filtrate solution was stored at 4 °C for further experiments.

2.3. Biological synthesis of the bT-ZnO NCs

To synthesize the bT-ZnO NCs, we followed our previously established protocol[11] based on a co-precipitation method. Consequently, 20 mM of 50 ml zinc acetate dihydrate aqueous solution was kept on magnetic stirring at 400 rpm, and after 10 min of stirring, *AN* plant extract was added in three lots (0.25, 0.5, and 1.0 ml). Further, after the addition of *AN* plant extract, it was left for 10 min stirring, with the pH maintained at 12 by using 2 M NaOH solution, and then it was left for 2 h stirring, ultimately resulting in a change of color from transparent to a yellow-colored precipitate, and slowly it turned into a white-colored precipitate. The precipitate was centrifuged at 10000 rpm for 5 min and washed three times with Milli-Q water. After washing three times, the white pellet was collected in a watch glass and placed in a hot air oven at 60 °C for 8 h drying. After air-drying, the synthesized bT-ZnO NCs were stored in an airtight container for further characterization and application.

2.4. Electrophoretic deposition of the bT-ZnO NCs on the ITO

This work will utilize the electrophoretic deposition (EPD) method to make a thin film of prepared bT-ZnO NCs. For performing EPD, a hydrolyzed ITO glass substrate (1 × 2 cm) was utilized. Further, after optimizing all the EPD parameters, 1 mg of prepared bT-ZnO NCs was added to a 20% ethanol–water mixture (20 ml), which underwent 30 min ultrasonication to form a colloidal dispersion. Further, for preparing the bT-ZnO/ITO electrode, 25 V current was applied for 1 min to form a uniform film, and the prepared electrode was used in the electro-oxidation studies of AA.

2.5. Characterization

UV-vis absorption spectroscopy was performed using a UV-1800 instrument (Shimadzu, Japan), in the wavelength range of 200–800 nm to investigate the optical properties of the NCs. The vibration spectrum of the synthesized biogenic bT-ZnO NCs was determined on an FTIR spectrophotometer (Nicolet iS5, Thermo Fisher Scientific) in the spectral range of 400–4000 cm^{-1}. XRD techniques were used to examine the structure and crystalline size of the bT-ZnO NCs on an X-ray diffractometer (D8 Advance, Bruker) with a Cu-Kα radiation ($\lambda = 1.5406$ Å) in the 2θ angles ranging from 10° to 80°. A Zetasizer instrument (Litesizer 500, Anton Paar) was used to determine the zeta potential of the synthesized materials. SEM and energy dispersive X-ray analysis (EDX) were performed to determine the surface morphology and element confirmation, respectively, of the synthesized NCs using an EVO 18 system (Zeiss, Germany). TEM analysis was performed for elemental imaging of the bT-ZnO NCs utilizing an FEI Tecnai G2 F20-Twin system (Swiss Republic), at an operating voltage of 300 kV. AFM (NEXT, NT-MDT) was used to determine the surface morphology of the

fabricated bT-ZnO/ITO electrodes. A Genetix DC power supply was used for performing EPD. Further, the electro-oxidation study of AA by the bT-ZnO/ITO electrode was performed using an electrochemical workstation (Kanopy Techno Solutions Pvt Ltd, India), using a three-electrode setup.

3. Result and discussion

3.1. Structural, optical, and morphological characterization of bT-ZnO NCs

Initially, the synthesized bT-ZnO NCs were analyzed with a UV-vis spectrophotometer between 200–600 nm scan range. The UV-vis spectral analysis confirmed the reduction of zinc acetate dihydrate to bT-ZnO NCs through the surface plasmon resonance (SPR) peak at 365 nm (Fig. 2A). The formation of the SPR absorption band may be due to the presence of free electrons and the interaction of the light wave with the free electrons of the bT-ZnO NCs.[34] The sharp peak present in the visible spectral analysis confirmed the uniformity in the biosynthesized ZnONPs. Moreover, the obtained UV-vis result is in good agreement with previous reports on zinc oxide nanoparticles using biogenic synthesis.[11] Further, a Tauc plot was used to calculate the energy band gap, as shown in Fig. 2B, and the measured band gap was 3.04 eV, as calculated by plotting the graph between energy *vs.* $(\alpha h\nu)^2$ (eV $cm^{-1})^2$. where α is the absorption coefficient, ν is the frequency of the incident rays, and h is Plank's constant.

FTIR study of the bT-ZnO NCs was performed for the wavenumber *vs.* transmittance to analyze the synthesized bT-ZnO NCs within a scan range of 4000–500 cm^{-1} to determine the phytochemicals responsible for the formation, capping, and stabilization of the biosynthesized zinc oxide nanoclusters from the nascent leaf extract of *AN*. The FTIR spectrum of the of bT-ZnO NCs showed major absorption peaks (Fig. 2C) at 3721, 3623, 2976, 2357, 2179, 2034, 1647, 1556, 1050, 1008, 673, 417, and 407 cm^{-1}. The spectra of the biosynthesized sample detected a peak at 3623 cm^{-1}, revealing the presence of an O–H hydroxyl of the alcohol, while the peak at 2976 cm^{-1} corresponded to the C–H stretching of the alkane functional groups. The strong absorption peak at 2357 cm^{-1} was assigned to the P–H of phosphine, while the absorption peak at 2034 cm^{-1} demonstrated the existence of N=C in R–N=C=S, whereas the absorption peak at 1556 cm^{-1} indicated the C–O stretch of the carboxylic group. The absorption peaks at 1647, 1050, 673, 417, and 407 cm^{-1} were associated with the vibration modes of the zinc oxide nanoparticles (metal–oxygen).[35–37] Furthermore, the slight variations in intensity at 3865–3760 cm^{-1} reflected the

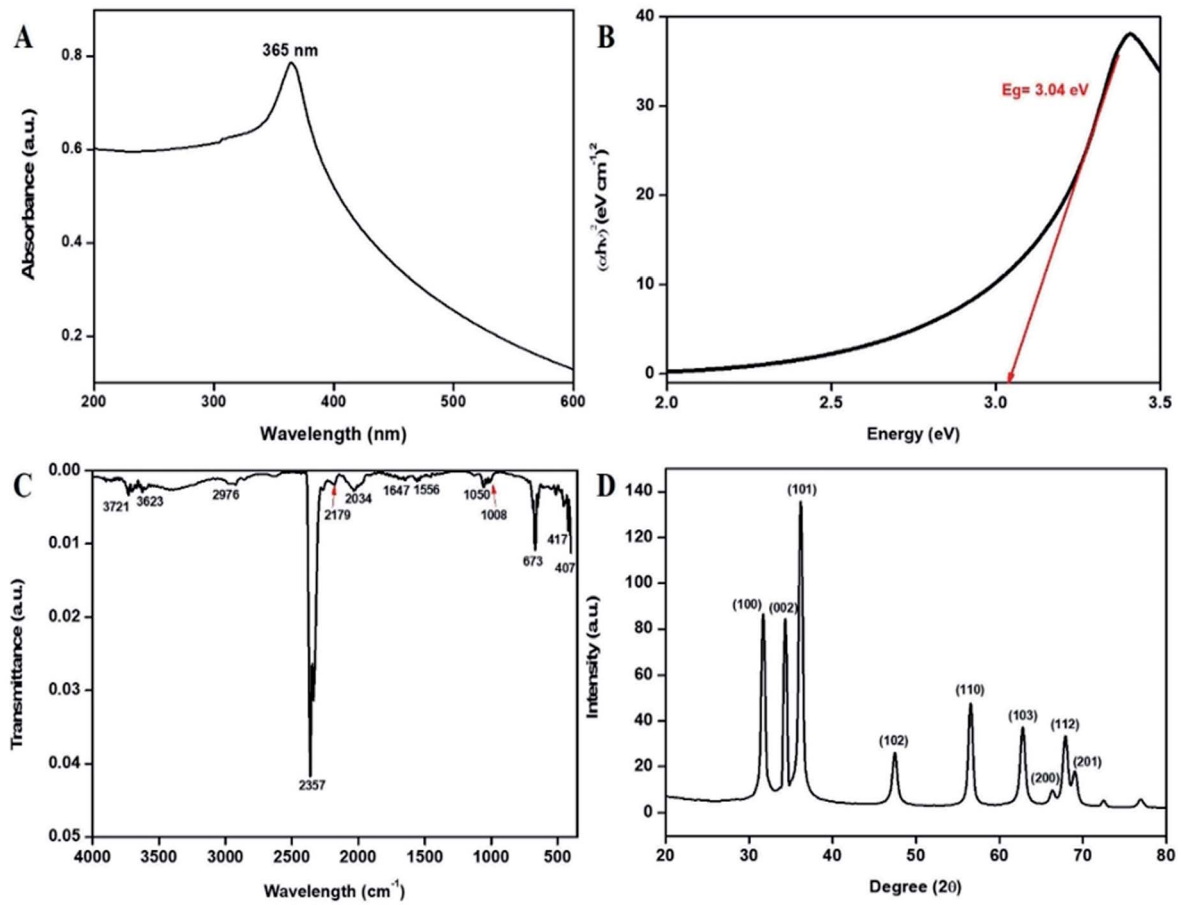

Fig. 2 (A) UV-vis absorption spectra of the bT-ZnO NCs, (B) Tauc plot demonstrating the energy band gaps, (C) FTIR vibration spectra of the bT-ZnO NCs, and (D) XRD pattern of the bT-ZnO NCs.

involvement of an intermediate form of phenolic groups, such as protein and carbohydrates. Further, the zeta potential analysis of the bT-ZnO NCs displayed a negative potential of −22 mV; from this, it can be stated that these bioinspired nanoclusters were highly bioactive and would remain stable in the colloidal suspension.

The X-ray diffraction (XRD) patterns revealed the orientation and crystalline nature of the bT-ZnO NCs (Fig. 2D). The peaks in the standing state for the 2θ values of 31.36, 34.41, 36.18, 47.43, 56.59, 62.78, 66.00, 67.98, and 69.00 were recorded as the (100), (002), (101), (102), (110), (103), (200), (112), and (201) planes, respectively, which were in good agreement with the International Centre of Diffraction Data card (JCPDS no. 89-1397) confirming the formation of bT-ZnO NCs, which were attributed to a hexagonal structure. Moreover, these diffraction peaks fitted well with the pure hexagonal phase of wurtzite bT-ZnO NCs in the space group $P6_3mc$ (no: 186), having the lattice parameters $a = 3.253$ and $c = 5.213$. Apart from this, no extra diffraction peaks of other phases were detected, indicating the purity of the bT-ZnO NCs. Further, the average crystallite size could be calculated using the Debye–Scherrer formula (eqn (1)) from the obtained crystallographic planes, and the calculated average crystalline size from eqn (2) was found to be 22 nm. In eqn (1), D corresponds to the crystallite size, the X-ray wavelength ($\lambda = 1.5406$ Å), β is the full width at half maximum (FWHM) of the more intense peak, and the Bragg diffraction angle is represented by θ.

$$D = 0.9\lambda/(\beta \cos \theta) \quad (1)$$

To investigate the bT-ZnO/ITO electrode's surface properties, atomic force microscopy (AFM) studies were carried out, and the results are demonstrated in Fig. 3A. The morphology of the bT-ZnO/ITO electrode showed a uniform distribution of bT-ZnO NCs on the ITO surface, while the roughness calculation for the ZnO electrode surface gave a root mean square roughness (RMS-R_q), roughness average (R_a), and max peak height profile of 29.024 nm, 16.974 nm, and 232.022 nm, respectively. The max peak height here is very high due to the trigonal morphology of the synthesized material. Further, it was also observed that the bT-ZnO NCs on the surface of ITO were distributed uniformly, and the distributed particles were trigonal, awhile the bT-ZnO/ITO electrodes 3D surface morphology also demonstrated the homogeneous distribution of the trigonal structure of ZnO. Further, the surface topology of the bT-ZnO NCs powder was validated by scanning electron microscopy (SEM; Fig. 3B), and it

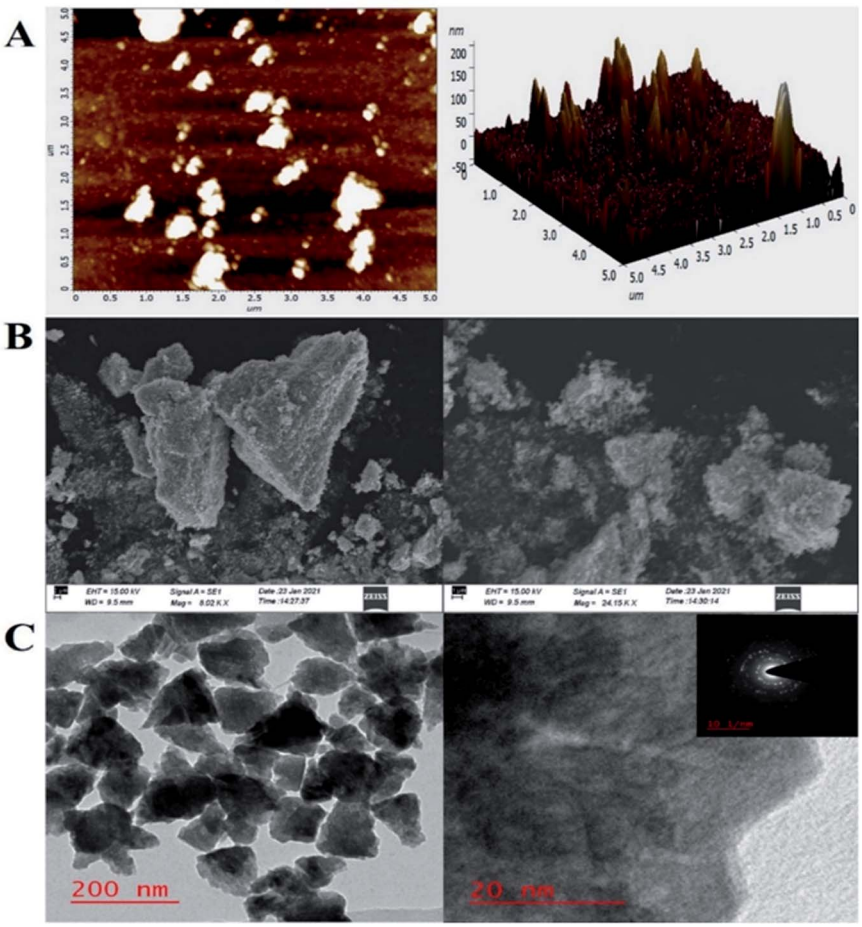

Fig. 3 AFM, SEM, and TEM analysis of the bT-ZnO NCs, (A) AFM data of the bT-ZnO/ITO electrode 2D (left), and 3D (right), (B) SEM micrography, and (C) TEM analysis: HR-TEM and inset the SAED analysis (right).

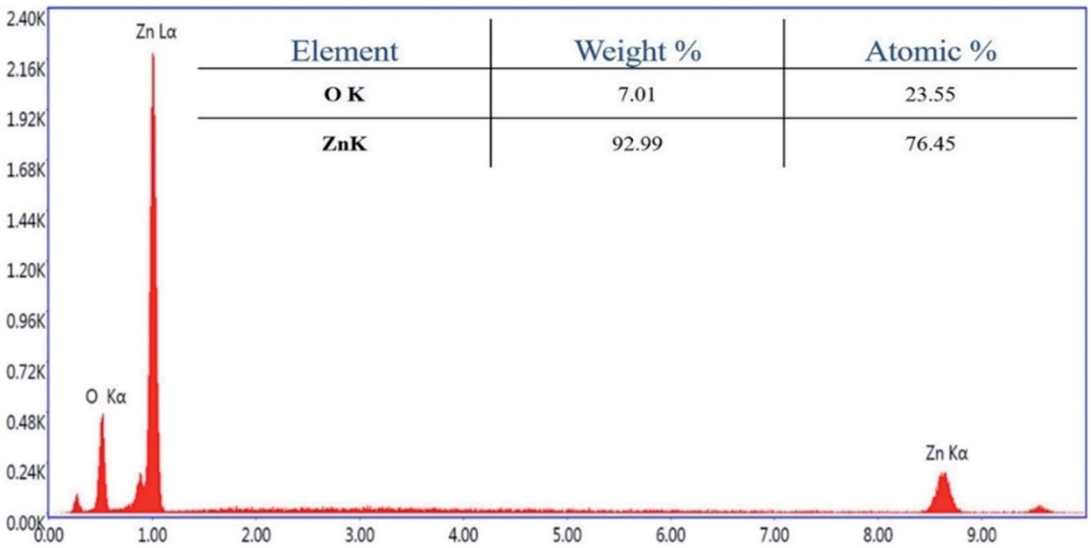

Element	Weight %	Atomic %
O K	7.01	23.55
ZnK	92.99	76.45

Fig. 4 bT-ZnO NCs' EDX analysis.

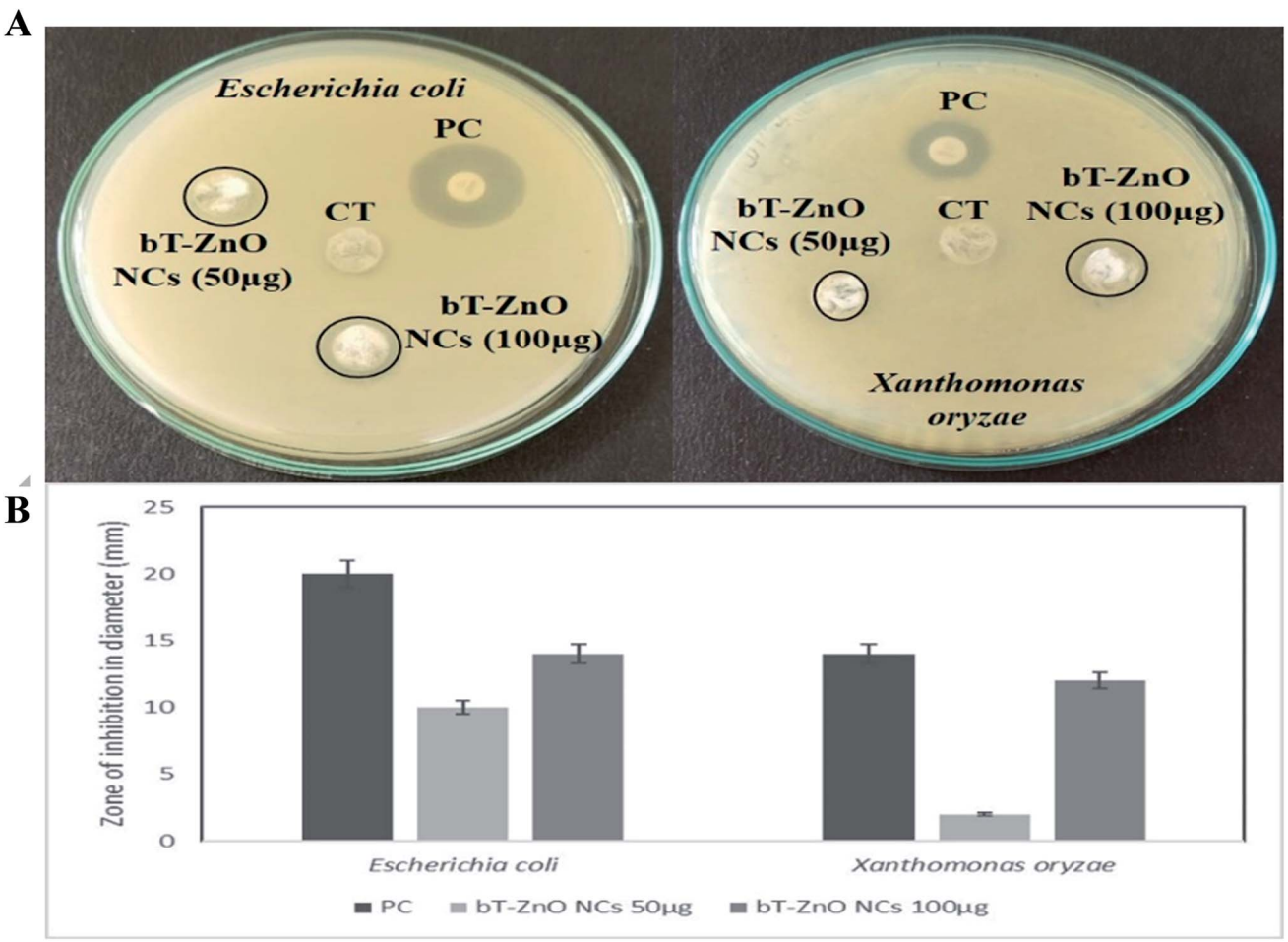

Fig. 5 Antibacterial activity of the bT-ZnO NCs: (A) well-diffusion antibacterial assay of bT-ZnO NCs for *Escherichia coli and Xanthomonas oryzae* bacterial strains, where, CT is the control (plant extract-AN); and PC is the positive control (ampicillin). (B) Zone of inhibition of the PC and different concentrations of bT-ZnO NCs (50 and 100 μg) on *E. coli* and *X. oryzae*.

demonstrated again that the bT-ZnO NCs had a trigonal shape and were uniformly distributed, as determined in relation to the obtained AFM data; however, agglomeration was also observed to some extent.

Further, transmission electron microscopy (TEM) analysis of the bT-ZnO NCs revealed the average particle size and shape, as demonstrated in Fig. 3C. The result revealed that most of the bT-ZnO NCs were trigonal, while the quantitative analysis performed by TEM revealed that the average particle size of the bT-ZnO NCs was around 43 nm, which was also determined by fitting the histogram by the Lorentzian function (not included in data form). Thus, the average particle size and crystalline particle size calculated by XRD were related, as the crystalline size of a particle can be ±20 nm less than the average particle size of NCs. In addition to this, the SAED (selected area electron diffraction) image (Fig. 3C) obtained from the TEM analysis was completely related to the 2θ peaks obtained in the XRD, while the SAED image also demonstrated the highly polycrystalline nature of the synthesized bT-ZnO NCs. To conclude, it was necessary to confirm the synthesized NCs elemental compositions, which were examined *via* EDX, and the obtained result demonstrated (Fig. 4) and confirmed that the synthesized NCs were ZnO, as EDX demonstrated the presence of only two elements Zn and O with atomic percentages of 76.45% and 23.55%, respectively.

3.2. Antibacterial studies

Crop plants are highly susceptible to various bacterial pathogens, which can lead to severe crop losses, potentially resulting in global socio-economic disturbance. Therefore, controlling plant diseases using antibacterial agents without affecting the environment is a pressing need in agriculture. In this work, we also hypothesized that the bT-ZnO NCs could act as a potential antibacterial agent for agricultural applications for combating various plant pathogenic bacteria. However herein in this work, we utilized a Gram-negative plant pathogenic bacteria, *X. oryzae*, a major host in rice (*Oryza sativa*), in which it causes bacterial blight and affects more than 70% of rice crops yearly. The major regions in which the rice crop is highly affected by this pathogen are Asia, the Caribbean, Latin America, and Africa's western coast.[38] To demonstrate the antibacterial activity of bT-ZnO NCs, it was examined on *Escherichia coli* and *Xanthomonas oryzae* through a well-diffusion method. The antibacterial well-diffusion assay was performed in triplicate, and the bT-ZnO NCs at both the tested concentrations (50 μg and 100 μg) exhibited a zone of inhibition (ZOI) against both *E. coli* and *X. oryzae*. At a concentration of 50 μg of bT-ZnO NCs, the ZOI against both *E. coli* and *X. oryzae* was 10 and 2 mm in diameter, respectively, and at a concentration of 100 μg of bT-ZnO NCs, the ZOI against both *E. coli* and *X. oryzae* was 14 and 12 mm in diameter (Fig. 5A and B). Thus, it was evident that the ZOI increases with the increase in NCs concentration. Hence, it was manifested that the bT-ZnO NCs have the potential to be utilized as an agent for combating bacterial blight disease caused by *X. oryzae*, but it must be subjected to further comparative studies with Gram-positive bacteria as well as undergoing studies related to the nanotoxicological aspects.

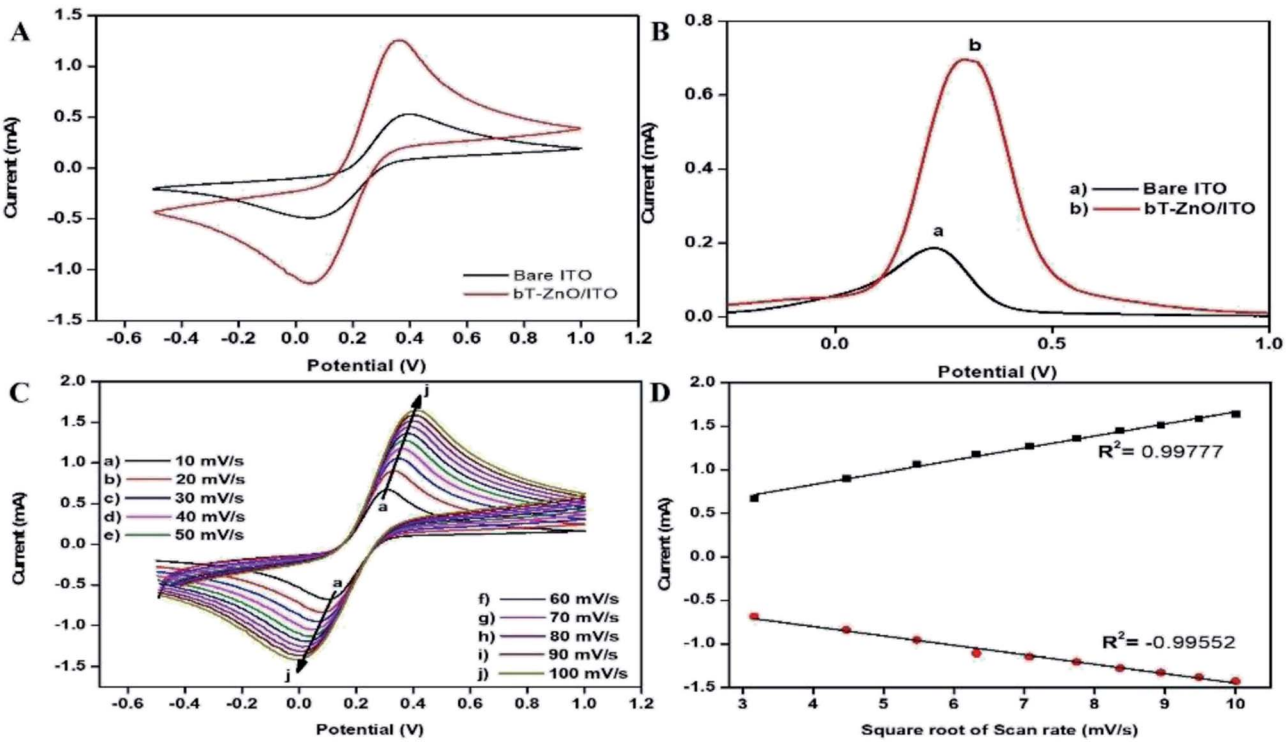

Fig. 6 (A) CV and (B) DPV of the bare ITO (black curve), and bT-ZnO/ITO (red curve), (C) CV curve of bT-ZnO/ITO at varying scan rates (10–100 mV s^{-1}, pH 7) at 27 °C. (D) Increasing current *vs.* difference in the potential as a function of the square root of the scan rate (10–100 mV s^{-1}).

3.3. Electrochemical studies

3.3.1. Cyclic voltammetry and differential pulse voltammetric studies. The redox behavior of the bT-ZnO/ITO electrodes prepared by EPD was investigated in 50 mM PBS (0.9% NaCl) solution of pH 7 containing 5 mM $[Fe(CN)_6]^{3-/4-}$ at a 50 mV s^{-1} scan rate, in comparison with the bare ITO electrode (Fig. 6A). The cyclic voltammetry (CV) of bare ITO (black curve) exhibited a redox couple of peaks, which corresponded to the mediator $[Fe(CN)_6]^{3-/4-}$, which demonstrates the material's electrochemical characteristics, and the bare ITO showed an oxidation/anodic current peak (I_{pa}) at 0.53 mA. For the electrodeposited bT-ZnO/ITO electrode, the I_{pa} value was highly elevated, leading to a current peak at 1.26 mA (red curve), which demonstrated that the bT-ZnO NCs provided the ITO with relatively better conductivity owing to their large surface area, which further indicated the enhanced electrocatalytic behavior compared to ITO as an electrode. The results from the differential pulse voltammetric (DPV) studies were completely related to the CV measurement, as it also exhibited a higher current on the bT-ZnO NCs fabricated electrode (Fig. 6B).

3.3.2. Scan rate effect. For investigating the interfacial kinetics of the bT-ZnO/ITO electrode, as a function of varying the scan rate from 10–100 mV s^{-1}, CV studies were conducted (Fig. 6C). From this study, it was observed that the magnitude of the anodic/oxidation (I_{pa}) and cathodic/reduction (I_{pc}) peaks current increased linearly with respect to increasing the scan rate (Fig. 6D). Further, it was also evident that with increasing the scan rate, the current at I_{pa} was shifted toward a more positive potential value, whereas the current at I_{pc} was shifted toward more negative potential, which suggested that the oxidation–reduction (redox) behavior involved a quasi-reversible process.

3.3.3. Kinetic studies. The charge transfer rate constant (K_s) value change obtained by surface modification of the ITO by the bT-ZnO NCs was calculated using eqn (2),[39] where F is the Faraday constant (96 485C mol^{-1}); R is the gas constant, which is 8.314 J mol^{-1} K^{-1}; m is a separation of the peak-to-peak (V); n corresponds to the number of electrons transferred, *i.e.*, 1; ν is the scan rate (50 mV), and T is 27 °C (room temperature). By employing all these values, K_s was determined for the bT-ZnO/ITO electrode as 0.6382 s^{-1}, which was attributed to the increased transfer of electrons owing to the higher catalytic activity of the bT-ZnO NCs. The shift in potential ($\Delta E_p = E_{pa}$(-anodic peak) $- E_{pc}$(cathodic peak)) exhibited a linear relationship with respect to the scan rate (Fig. 6D). From this result, it is evident that the electrochemical reaction of AA with bT-ZnO NCs was a diffusion-controlled process. Further, the D (diffusion coefficient) for the diffusion of $[Fe(CN)_6]^{3-/4-}$ from the electrolyte solution to the bT-ZnO/ITO electrode surface was calculated by the Randles–Sevcik equation, eqn (3),[39] in which I_p corresponds to the electrode peak current, *i.e.*, I_{pa} and I_{pc}; n is the electron number (1); A is the electrode's surface area (0.25 cm^2); and C is the concentration at the surface in mol cm^{-3} (5 mM). Putting the values in eqn (3), the obtained D value of the bT-ZnO/ITO electrode was 2.0627×10^1 cm^2 s^{-1}. Moreover, the surface concentration of the electrode was projected by the Brown–Anson model (eqn (4)), where n is the electron transferred, *i.e.*, 1; γ corresponds to the electrode's surface concentration (mol cm^{-2}); and T is room temperature. Thus, the bT-ZnO/ITO's surface concentration was calculated by putting all the above values in to eqn (4) and was found to be 5.94×10^{-7} mol cm^{-2}.

$$K_s = mnF\nu/RT \quad (2)$$

$$I_p = (2.69 \times 10^5)n^{3/2}AD^{1/2}C\nu^{1/2} \quad (3)$$

$$I_p = n^2F^2\gamma AV/4RT \quad (4)$$

3.3.4. Optimization of the pH. The electrochemical behavior of bT-ZnO/ITO was optimized for different pHs (5.7 to 8.0) by CV studies in 50 mM PBS (0.9% NaCl) containing 5 mM

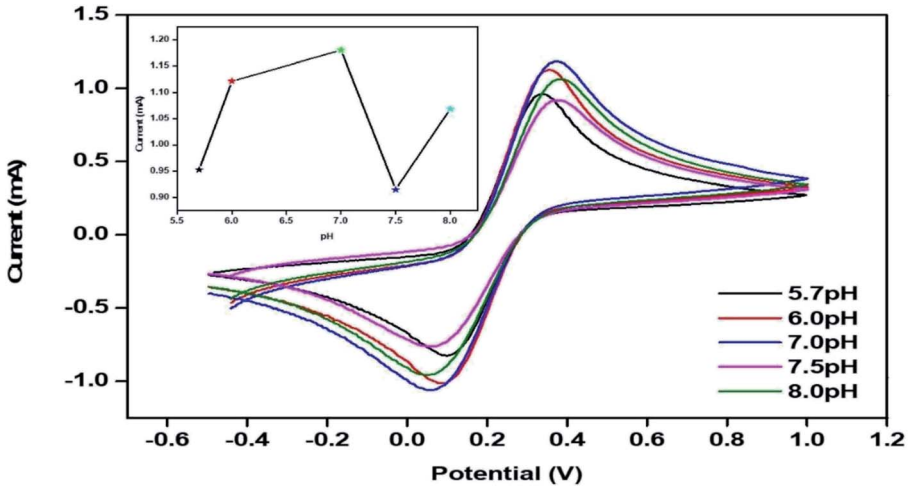

Fig. 7 CV of the bT-ZnO/ITO electrode with varying the pH (5.7 to 8) of 50 mM PBS (0.9% NaCl) containing 5 mM $[Fe(CN)_6]^{3-/4-}$; the inset shows the current response of the bT-ZnO/ITO electrode as a function of the pH.

$Fe[(CN)_6]^{3-/4-}$ at a scan rate of 50 mV s^{-1} (Fig. 7). It was observed that the oxidation/anodic peak current increased from pH 5.7 to 7, and then from pH 7, it again decreased up to 7.5 pH, and at pH 8, the I_{pa} value again increased slightly. The maximum current at I_{pa} was observed at pH 7 due to the interaction between the bT-ZnO/ITO with the $[Fe(CN)_6]^{3-/4-}$ when compared to the I_{pa} value of bT-ZnO/ITO at other pH conditions. Hence, pH 7 was considered a suitable pH for performing the CV measurements after optimization.

3.3.5. Electro-oxidation studies of AA. In this work here, we hypothesized that the bT-ZnO NCs have potential applications in the agricultural domain, and to prove this hypothesis, we demonstrated their electrochemical sensing response for AA, as under stress conditions plants secrete AA for combating stress. Thus, there is an urgent need to develop a highly effective sensor for determining plants' chemicals during stress conditions, which can help monitor plant stress conditions. For achieving this objective, the CV response of the bT-ZnO/ITO electrode was analyzed with different AA concentrations, in 50 mM PBS (pH 7, 0.9% NaCl) containing $[Fe(CN)_6]^{3-/4-}$ at a 50 mV s^{-1} scan rate. Fig. 8A shows the electrochemical sensing results by the CV of the bT-ZnO/ITO electrode as a function of varying the AA concentration (4 to 28 mM). From the CV studies, it was evident that with increasing the AA concentration, the anodic and cathodic peak current increased and decreased, respectively, at a linear interval, suggesting that the bT-ZnO NCs were very sensitive to AA. The overall redox reaction of AA by the bT-ZnO/ITO electrode is demonstrated in Fig. 9A and B.

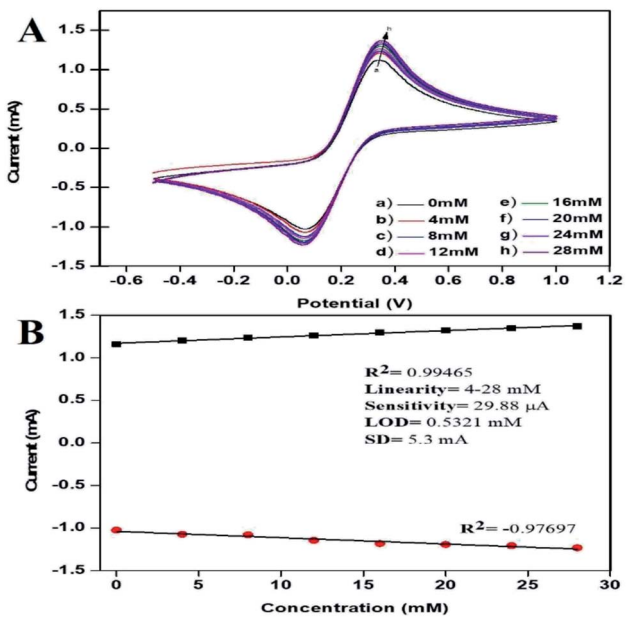

Fig. 8 (A) Electrochemical sensing of AA with varying the concentration (4–28 mM) by the bT-ZnO/ITO electrode in 50 mM PBS (pH 7, 0.9% NaCl) containing 5 mM $[Fe(CN)_6]^{3-/4-}$ at scan rate of 50 mV s^{-1}. (B) Calibration curve of the bT-ZnO/ITO electrode with varying the current as a function of the AA concentration (4–28 mM) in 50 mM PBS (pH 7, 0.9% NaCl) containing 5 mM $[Fe(CN)_6]^{3-/4-}$ at a scan rate of 50 mV s^{-1}.

The peak current obtained for the anodic/oxidation and cathodic/reduction peak showed a linear relationship with the concentration in the range between 4–28 mM (Fig. 8B). The linear calibration coefficient (R^2) obtained was 0.99465, demonstrating a strong relationship between the AA concentration and the obtained anodic/oxidation current. The fabricated bT-ZnO/ITO electrode showed a very low limit of detection (LOD) of 0.5321 mM and demonstrated linearity from 4–28 mM. Moreover, the fabricated electrode had a sensitivity of 29.88 μA, which suggested it was highly sensitive. The LOD was calculated by 3 × SD/sensitivity, where SD stands for the standard deviation of the calibration plot slope and the background current. From the bT-ZnO/ITO electrode's electro-oxidation activity results when exposed to various AA concentrations, it could be concluded that this electrode can be used as a prominent sensor for the quantitative determination of AA in agricultural samples as well as in biological samples too. For determination of the response time of the bT-ZnO/ITO electrode, the electrochemical response was measured from 0–60 seconds, and initially the current magnitude increased and reached a maximum value at 5 s, and after this, the current became saturated, which demonstrates that 5 s was the response time of the bT-ZnO/ITO electrode for the proper sensing of AA. Moreover, reproducibility/reusability studies were also performed (ESI Fig. 1A†), which demonstrated that after 25 scans, the bT-ZnO/ITO electrode lost only 1.52% of the current, demonstrating that this label-free electrode was highly reusable/reproducible. Furthermore, the stability or durability studies (ESI Fig. 1B†) were also performed for 46 days at an interval of 5 days, and the bT-ZnO/ITO electrode retained its activity for up to 46 days, as on the 46th day it had only lost 3.7% current, which justifies that the as-fabricated electrode was highly stable for up to 46 days at 4 °C. Further, Table 1 compares this results in this work for the electrochemical sensing of AA with the pre-existing works of this type with different materials as the electrode.[40–43]

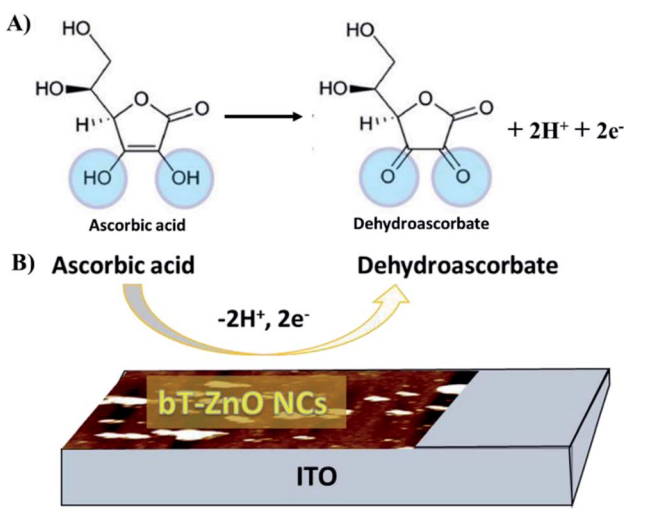

Fig. 9 Illustration of the redox reaction mechanism of AA: (A) general reaction of AA and (B) reaction mechanism of the AA redox reaction at the bT-ZnO/ITO electrode.

Table 1 Comparison of the electro-analytical parameters of previous works with this work

Method	Electrode	Medium pH	Sensitivity	Liner range	Detection limit	Response time	Ref.
CV	DPSA-doped nanoPANI/SPE	6.8 pH	10.75 μA mM^{-1}	0.5–8 mM	8.3 mM	—	40
CV	Polyaniline (PANI)/SCPE	5.0 pH	17.7 μA μM^{-1}	30–270 μM	30 μM	—	41
DPV	Au-PEDOT	7.0 pH	0.875 μA μM^{-1}	5–300 μM	2.5 μM	—	42
CV	Tm_2O_3/ITO electrode	7.0 pH	—	0.2–8 mM	0.42 mM	—	43
CV	bT-ZnO/ITO electrode	7.0 pH	29.88 μA mM^{-1}	4–28 mM	0.532 mM	5 seconds	Present work

It can be seen that the sensitivity and the response time obtained in this work are very promising when compared to other works.

4. Conclusion and future prospects

In this work, bioinspired triangular ZnO nanoclusters were characterized for their optical, structural, and morphological properties and then further investigated for their applications in the agricultural domain by checking the bT-ZnO NCs utility as an antibacterial agent for combating plant pathogenic bacterium and for utilization of the bT-ZnO NCs for the label-free quantitative determination of AA in plants for the proper monitoring of plant stress conditions. The synthesized bT-ZnO NCs were found to be very advantageous when compared with other previously synthesized ZnO materials. In particular, the bT-ZnO NCs in this work could be synthesized from a single-step process by using plant extract as a capping, reducing, and stabilizing agent, which in turn make these synthesized NCs very cost-effective as the fabrication process does not utilizes any chemical or physical methods, which are generally expensive methods that are also harmful to the environment and need a high energy consumption. Thus, the bioinspired synthesis route utilizing plant extracts is suggested to be a possible environmentally friendly alternative over chemical and physical methods and offers enhanced stability for the synthesized material, improved environmental friendliness, and a higher yield.

Moreover, in this work, we performed preliminary studies to prove the utility of the bT-ZnO NCs as an antibacterial agent, and the results proved that the bT-ZnO NCs were highly beneficial for combating bacterial blight disease in the rice crop, but still more studies related to comparisons between Gram-negative and Gram-positive bacteria are needed as well as nanotoxicological studies of the bT-ZnO NCs before utilization of this material on-field for combating bacterial blight disease. These remain our next objective. Moreover, herein we also reported the role of bT-ZnO NCs for their electro-oxidation response toward AA, which was demonstrated to show a very good response time, high sensitivity, and low LOD of 5 s, 29.88 μA, and 0.5321 mM, respectively. The sensing of AA was highly linear in the range from 4–28 mM. Thus, this study's findings demonstrate that the bT-ZnO NCs are a promising agent to be utilized in agriculture as an antibacterial agent for combating bacterial blight disease in rice crops and also may be a capable platform for the label-free, simple, and rapid quantitative determination of AA in agricultural samples of plants/crops, for proper monitoring of plants under stress conditions. Further, from the results of this study, the ZnO-based AA sensors can be a prominent tool for determining the AA levels in plants. The work reported herein represents preliminary information, and we are also continuing to work on these models for the commercial availability of our bT-ZnO NCs-based sensors for the on-field detection of AA, although currently, we are first working toward the further optimization of this sensor for making it cost-effective, robust, and more accurate. To achieve this, we are working on the fabrication of a paper-based electrode with the same material to achieve a similar/higher sensitivity and effectiveness for making this technology more cost effective.

Author contributions

PS: contributed to the data curation, investigation, resources, validation, and writing the original draft. KRBS: contributed to the conceptualization, data curation, investigation, resources, validation, writing the original draft and reviewing & editing the manuscript draft. JS: contributed to the data curation, resources, supervision, visualization, writing the original draft, and editing the manuscript draft. PP: contributed to the data curation, validation, and writing the manuscript draft. RPS: contributed to the conceptualization, data curation, validation, project administration, supervision, writing the original draft, and reviewing & editing the manuscript draft.

Conflicts of interest

The authors declare no conflict of interest for this work.

Acknowledgements

PS is thankful to the Ministry of Tribal Affairs, Government of India, for providing fellowship to carry out this work. KRBS would like to express their gratitude of thanks to Dr Rishi Paliwal (Department of Pharmacy, IGNTU, Amarkantak) and Professor Rajiv Prakash (IIT-BHU, Varanasi) for helping in the characterization of the synthesized materials; he is also thankful to Professor A. K. Singh for providing constant support and guidance throughout this work. JS expresses their gratitude of thanks to the DST-INSPIRE faculty Fellowship, BHU (IoE grant), and UGC New Delhi for financial support. PP thanks Dr Subha Narayan Das, Department of Botany, IGNTU,

Amarkantak, for providing constant support and guidance, and RPS is thankful to VC, IGNTU, Amarkantak, India, for providing constant support financially and for motivating us to do good science.

References

1 T. Tuutijärvi, J. Lu, M. Sillanpää and G. Chen, As(v) adsorption on maghemite nanoparticles, *J. Hazard. Mater.*, 2009, **166**, 1415–1420, DOI: 10.1016/j.jhazmat.2008.12.069.

2 K. Tanabe, Optical radiation efficiencies of metal nanoparticles for optoelectronic applications, *Mater. Lett.*, 2007, **61**, 4573–4575, DOI: 10.1016/j.matlet.2007.02.053.

3 H. Zhang, Y. Liu and S. Sun, Synthesis and assembly of magnetic nanoparticles for information and energy storage applications, *Front. Phys.*, 2010, **5**, 347–356, DOI: 10.1007/s11467-010-0104-9.

4 D. R. Bhumkar, H. M. Joshi, M. Sastry and V. B. Pokharkar, Chitosan Reduced Gold Nanoparticles as Novel Carriers for Transmucosal Delivery of Insulin, *Pharm. Res.*, 2007, **24**, 1415–1426, DOI: 10.1007/s11095-007-9257-9.

5 A. K. Mittal, Y. Chisti and U. C. Banerjee, Synthesis of metallic nanoparticles using plant extracts, *Biotechnol. Adv.*, 2013, **31**, 346–356, DOI: 10.1016/j.biotechadv.2013.01.003.

6 I. Willner, R. Baron and B. Willner, Growing Metal Nanoparticles by Enzymes, *Adv. Mater.*, 2006, **18**, 1109–1120, DOI: 10.1002/adma.200501865.

7 A. K. Jha, K. Prasad and A. R. Kulkarni, Synthesis of TiO_2 nanoparticles using microorganisms, *Colloids Surf., B*, 2009, **71**, 226–229, DOI: 10.1016/j.colsurfb.2009.02.007.

8 M. Jain, R. Kapadia, R. N. Jadeja, M. C. Thounaojam, R. V. Devkar and S. H. Mishra, Traditional uses, phytochemistry and pharmacology of Tecomella undulata – A review, *Asian Pac. J. Trop. Biomed.*, 2012, **2**, S1918–S1923, DOI: 10.1016/S2221-1691(12)60521-8.

9 V. Kumar and S. K. Yadav, Plant-mediated synthesis of silver and gold nanoparticles and their applications, *J. Chem. Technol. Biotechnol.*, 2009, **84**, 151–157, DOI: 10.1002/jctb.2023.

10 R. P. Singh, Nanobiosensors: Potentiality towards Bioanalysis, *J. Bioanal. Biomed.*, 2016, **8**(4), 1000e143, DOI: 10.4172/1948-593X.1000e143.

11 R. P. Singh, V. K. Shukla, R. S. Yadav, P. K. Sharma, P. K. Singh and A. C. Pandey, Biological Approach Of Zinc Oxide Nanoparticles Formation And Its Characterization, *Adv. Mater. Lett.*, 2011, **2**, 313–317, DOI: 10.5185/amlett.indias.204.

12 R. P. Singh, Application of Nanomaterials Toward Development of Nanobiosensors and Their Utility in Agriculture, in *Nanotechnology*, Springer Singapore, Singapore, 2017, pp. 293–303. DOI: 10.1007/978-981-10-4573-8_14.

13 S. Mallakpour, E. Azadi and C. Mustansar Hussain, Environmentally benign production of cupric oxide nanoparticles and various utilizations of their polymeric hybrids in different technologies, *Coord. Chem. Rev.*, 2020, **419**, 213378, DOI: 10.1016/j.ccr.2020.213378.

14 M. Anbuvannan, M. Ramesh, G. Viruthagiri, N. Shanmugam and N. Kannadasan, Anisochilus carnosus leaf extract mediated synthesis of zinc oxide nanoparticles for antibacterial and photocatalytic activities, *Mater. Sci. Semicond. Process.*, 2015, **39**, 621–628, DOI: 10.1016/j.mssp.2015.06.005.

15 R. Dobrucka and J. Długaszewska, Biosynthesis and antibacterial activity of ZnO nanoparticles using trifolium pratense flower extract, *Saudi J. Biol. Sci.*, 2016, **23**, 517–523, DOI: 10.1016/j.sjbs.2015.05.016.

16 J. Y. Song, H.-K. Jang and B. S. Kim, Biological synthesis of gold nanoparticles using Magnolia kobus and Diopyros kaki leaf extracts, *Process Biochem.*, 2009, **44**, 1133–1138, DOI: 10.1016/j.procbio.2009.06.005.

17 K. R. B. Singh, V. Nayak, T. Sarkar and R. P. Singh, Cerium oxide nanoparticles: properties, biosynthesis and biomedical application, *RSC Adv.*, 2020, **10**, 27194–27214, DOI: 10.1039/d0ra04736h.

18 V. Nayak, K. R. Singh, A. K. Singh and R. P. Singh, Potentialities of selenium nanoparticles in biomedical science, *New J. Chem.*, 2021, **45**, 2849–2878, DOI: 10.1039/d0nj05884j.

19 M. Fernandes, Recent Applications Of Magnesium Oxide (MgO) Nanoparticles In Various Domains, *Adv. Mater. Lett.*, 2020, **11**, 20081543, DOI: 10.5185/amlett.2020.081543.

20 R. P. Singh, *Potential of Biogenic Plant-Mediated Copper and Copper Oxide Nanostructured Nanoparticles and Their Utility*, 2019, pp. 115–176. DOI: 10.1007/978-3-030-16379-2_5.

21 P. A. R. Ashutosh Meher and A. Anuji Kumar, A Literature Review on *Argyreia nervosa* (Burm. F.) Bojer, *Int. J. Res. Ayurveda Pharm.*, 2011, **2**, 1501–1504.

22 A. K. Lykkeberg, J. Christensen, B. A. Budnik, F. Abe and J. W. Jaroszewski, In Vitro Cytotoxic Activity of Phenanthroindolizidine Alkaloids from Cynanchum v incetoxicum and Tylophora t anakae against Drug-Sensitive and Multidrug-Resistant Cancer Cells, *J. Nat. Prod.*, 2002, **65**, 1299–1302, DOI: 10.1021/np0106384.

23 Y. Bansal and A. Bharati, Phytochemical investigation of natural and *in vitro* raised Vrddhadaruka plants, *Anc. Sci. Life*, 2014, **34**, 80, DOI: 10.4103/0257-7941.153463.

24 G. D. Saratale, R. G. Saratale, G. Benelli, G. Kumar, A. Pugazhendhi, D.-S. Kim and H.-S. Shin, Anti-diabetic Potential of Silver Nanoparticles Synthesized with *Argyreia nervosa* Leaf Extract High Synergistic Antibacterial Activity with Standard Antibiotics Against Foodborne Bacteria, *J. Cluster Sci.*, 2017, **28**, 1709–1727, DOI: 10.1007/s10876-017-1179-z.

25 W. Maret, Metals on the move: zinc ions in cellular regulation and in the coordination dynamics of zinc proteins, *BioMetals*, 2011, **24**, 411–418, DOI: 10.1007/s10534-010-9406-1.

26 H. Tapiero and K. D. Tew, Trace elements in human physiology and pathology: zinc and metallothioneins, *Biomed. Pharmacother.*, 2003, **57**, 399–411, DOI: 10.1016/S0753-3322(03)00081-7.

27 Z. Fan and J. G. Lu, Zinc Oxide Nanostructures: Synthesis and Properties, *J. Nanosci. Nanotechnol.*, 2005, **5**, 1561–1573, DOI: 10.1166/jnn.2005.182.

28 M. Cassandri, A. Smirnov, F. Novelli, C. Pitolli, M. Agostini, M. Malewicz, G. Melino and G. Raschellà, Zinc-finger proteins in health and disease, *Cell Death Discovery*, 2017, **3**, 17071, DOI: 10.1038/cddiscovery.2017.71.

29 A. N. El-Shazly, M. M. Rashad, E. A. Abdel-Aal, I. A. Ibrahim, M. F. El-Shahat and A. E. Shalan, Nanostructured ZnO photocatalysts prepared *via* surfactant assisted Co-precipitation method achieving enhanced photocatalytic activity for the degradation of methylene blue dyes, *J. Environ. Chem. Eng.*, 2016, **4**, 3177–3184, DOI: 10.1016/j.jece.2016.06.018.

30 M. F. Sanad, A. E. Shalan, S. M. Bazid and S. M. Abdelbasir, Pollutant degradation of different organic dyes using the photocatalytic activity of ZnO@ZnS nanocomposite materials, *J. Environ. Chem. Eng.*, 2018, **6**, 3981–3990, DOI: 10.1016/j.jece.2018.05.035.

31 M. F. Sanad, E. S. Abu Serea, S. M. Bazid, S. Nabih, M. A. Ahsan and A. E. Shalan, High cytotoxic activity of ZnO@leucovorin nanocomposite based materials against an MCF-7 cell model, *Anal. Methods*, 2020, **12**, 2176–2184, DOI: 10.1039/d0ay00498g.

32 X. Wang, Y. Ding, C. J. Summers and Z. L. Wang, Large-Scale Synthesis of Six-Nanometer-Wide ZnO Nanobelts, *J. Phys. Chem. B*, 2004, **108**, 8773–8777, DOI: 10.1021/jp048482e.

33 T. Jamieson, R. Bakhshi, D. Petrova, R. Pocock, M. Imani and A. M. Seifalian, Biological applications of quantum dots, *Biomaterials*, 2007, **28**, 4717–4732, DOI: 10.1016/j.biomaterials.2007.07.014.

34 K. Sri Sindhura, T. N. V. K. V. Prasad, P. Panner Selvam and O. M. Hussain, Synthesis, characterization and evaluation of effect of phytogenic zinc nanoparticles on soil exo-enzymes, *Appl. Nanosci.*, 2014, **4**, 819–827, DOI: 10.1007/s13204-013-0263-4.

35 L. Patrón-Romero, P. A. Luque, C. A. Soto-Robles, O. Nava, A. R. Vilchis-Nestor, V. W. Barajas-Carrillo, C. E. Martínez-Ramírez, J. R. Chávez Méndez, J. A. Alvelais Palacios, M. Á. Leal Ávila and H. Almanza-Reyes, Synthesis, characterization and cytotoxicity of zinc oxide nanoparticles by green synthesis method, *J. Drug Delivery Sci. Technol.*, 2020, **60**, 101925, DOI: 10.1016/j.jddst.2020.101925.

36 H. Kumar and R. Rani, Structural and Optical Characterization of ZnO Nanoparticles Synthesized by Microemulsion Route, *Int. Lett. Chem., Phys. Astron.*, 2013, **19**, 26–36, DOI: 10.18052/www.scipress.com/ilcpa.19.26.

37 A. Sachdeva, S. Singh and P. K. Singh, Effect of incorporation of zinc oxide nanoparticles on properties of PEMA based polymer electrolyte, *Mater. Today: Proc.*, 2021, **34**, 697–701, DOI: 10.1016/j.matpr.2020.03.707.

38 H. Yen, *Rice bacterial blight, Encycl. Br.*, 2020, https://www.britannica.com/science/rice-bacterial-blight, accessed February 15, 2021.

39 P. Singh, K. R. Singh, J. Singh, S. N. Das and R. P. Singh, Tunable electrochemistry and efficient antibacterial activity of plant-mediated copper oxide nanoparticles synthesized by annona squamosa seed extract for agricultural utility, *RSC Adv.*, 2021, **11**, 18050–18060, DOI: 10.1039/d1ra02382a.

40 A. Ambrosi, A. Morrin, M. R. Smyth and A. J. Killard, The application of conducting polymer nanoparticle electrodes to the sensing of ascorbic acid, *Anal. Chim. Acta*, 2008, **609**, 37–43, DOI: 10.1016/j.aca.2007.12.017.

41 W. Kit-Anan, A. Olarnwanich, C. Sriprachuabwong, C. Karuwan, A. Tuantranont, A. Wisitsoraat, W. Srituravanich and A. Pimpin, Disposable paper-based electrochemical sensor utilizing inkjet-printed polyaniline modified screen-printed carbon electrode for ascorbic acid detection, *J. Electroanal. Chem.*, 2012, **685**, 72–78, DOI: 10.1016/j.jelechem.2012.08.039.

42 F. Sekli-Belaidi, P. Temple-Boyer and P. Gros, Voltammetric microsensor using PEDOT-modified gold electrode for the simultaneous assay of ascorbic and uric acids, *J. Electroanal. Chem.*, 2010, **647**, 159–168, DOI: 10.1016/j.jelechem.2010.06.007.

43 J. Singh, M. Srivastava, A. Roychoudhury, D. W. Lee, S. H. Lee and B. D. Malhotra, Optical and electrocatalytic studies of nanostructured thulium oxide for vitamin C detection, *J. Alloys Compd.*, 2013, **578**, 405–412, DOI: 10.1016/j.jallcom.2013.06.026.